ARTICLES
https://doi.org/10.1038/s41561-019-0398-3
nature geoscience

Early Moon formation inferred from hafnium–tungsten systematics

Maxwell M. Thiemens[1,4*], Peter Sprung[1,2], Raúl O. C. Fonseca[1], Felipe P. Leitzke[3,5] and Carsten Münker[1]

The date of the Moon-forming impact places an important constraint on Earth's origin. Lunar age estimates range from about 30 Myr to 200 Myr after Solar System formation. Central to this age debate is the greater abundance of ^{182}W inferred for the silicate Moon than for the bulk silicate Earth. This compositional difference has been explained as a vestige of less late accretion to the Moon than to the Earth after core formation. Here we present high-precision trace element composition data from inductively coupled plasma mass spectrometry for a wide range of lunar samples. Our measurements show that the Hf/W ratio of the silicate Moon is higher than that of the bulk silicate Earth. By combining these data with experimentally derived partition coefficients, we found that the ^{182}W excess in lunar samples can be explained by the decay of the now extinct ^{182}Hf to ^{182}W. ^{182}Hf was only extant for the first 60 Myr after the Solar System formation. We conclude that the Moon formed early, approximately 50 Myr after the Solar System, and that the excess ^{182}W of the silicate Moon is unrelated to late accretion.

The Moon probably formed in the aftermath of a giant impact between the proto-Earth and an erstwhile planetary body[1]. Extreme chemical and isotopic similarities between the Earth and the Moon[2] led to a growing consensus that they share a common chemical ancestry. This similarity in chemical signatures implies either that the bulk silicate Earth (BSE) is the major source of Moon-forming impact debris[3–6] or that the proto-Earth and the impactor had virtually identical chemical compositions[6]. Beyond chemical constraints on the Moon-forming giant impact event, there is an ongoing controversy as to its exact timing—some researchers argue that the Moon formed early (that is, 30–100 Myr after Solar System formation (SSF))[7–12], whereas others contend the Moon formed up to 200 Myr after SSF[13–17]. To constrain lunar formation requires knowledge of the crystallization age of the lunar magma ocean (LMO), a product of the Moon's high-energy impact formation. Central to the lunar age controversy are small excesses in the ^{182}W abundance in lunar basalts when compared to those on Earth, which average a value of +25 μ^{182}W units[18–20]. To assume that the excess ^{182}W in lunar samples stems from the in situ decay of short-lived ^{182}Hf to ^{182}W (8.9 Myr half-life[21]) places the lunar formation between 30 and 60 Myr after the SSF when sufficient ^{182}Hf was still present. However, this interpretation is at odds with the apparent observation that the BSE and the silicate Moon have virtually overlapping ratios of Hf (mother) to W (daughter), with Hf/W ratios of 24.9 and 25.8, respectively[22,23]. These seemingly identical parent-to-daughter ratios imply that their different μ^{182}W values cannot be related to the in situ decay of ^{182}Hf. Hence, an alternative explanation invoked that the Earth and Moon received a disproportionate contribution of late-accretion components with a chondritic Hf/W ratio (~1) and lower ^{182}W than that of BSE[19]. As the Moon is less massive than Earth, it would have received a commensurately smaller contribution from late accretion, and thus retained a higher μ^{182}W than BSE[18–20]. The Moon, therefore, constitutes a suitable highly siderophile-element-poor end member in such late-accretion models and a possible analogue to a proto-Earth that was essentially devoid of late-accretion components[20]. In addition to this view, the apparent decrease in ^{182}W values measured in terrestrial rocks over geological time has been explained by the protracted mixing of late veneer material into the terrestrial mantle that lowered μ^{182}W to its present-day value[12,20,24,25]. The presence of negative ^{182}W anomalies in Archaean samples, however, precludes the origin of the ^{182}W excess entirely from late accretion[26]. Often, the ^{182}W anomalies that have been found are coupled with ^{142}Nd anomalies, which is a decay product of ^{146}Sm, both lithophile elements[24,26–29], which makes it likely that ^{182}W excesses are the result of early silicate-differentiation events[30].

Any interpretation of lunar ^{182}W data relies on an accurate knowledge of the Hf/W ratio in lunar mantle reservoirs and by inference of the silicate Moon. Unfortunately, lunar Hf-W systematics are poorly constrained, as data of sufficient precision are scarce. This also extends to other highly incompatible elements (for example, the high field strength elements (HFSEs) U and Th) that are commonly used as proxies for W behaviour during dry terrestrial mantle melting[23]. In previous lunar studies[31], W was treated as a perfectly incompatible element (that is, having a similar behaviour as U or Th) during lunar differentiation. This treatment might be incorrect, as lunar mantle melting occurs under more reducing conditions than in the terrestrial mantle, implying that W may behave less incompatibly than elements like U and Th (refs. [32–34]). In fact, previous observations show that ratios of W with U or Th appear to be variable in lunar samples, which suggests that W behaves differently to highly incompatible elements like U or Th during lunar magmatism[31], in agreement with recent experimental studies[32–34].

Apollo sample results

To provide robust constraints on the Hf/W ratio value of the silicate Moon, we performed high-precision concentration measurements of W, Th, U and other HFSEs by isotope dilution on a representative

[1]Institut für Geologie und Mineralogie, Universität zu Köln, Köln, Germany. [2]Hot Laboratory Division (AHL), Paul Scherrer Institut, Villigen, Switzerland. [3]Steinmann Institut, Universität Bonn, Bonn, Germany. [4]Present address: Laboratoire G-Time, Département Géosciences, Environnement et Société, Université Libre de Bruxelles, Brussels, Belgium. [5]Present address: Isotope Geology Laboratory, Universidade Federal do Rio Grande do Sul, Porto Alegre, Brazil. *e-mail: Maxwell.Thiemens@ulb.ac.be

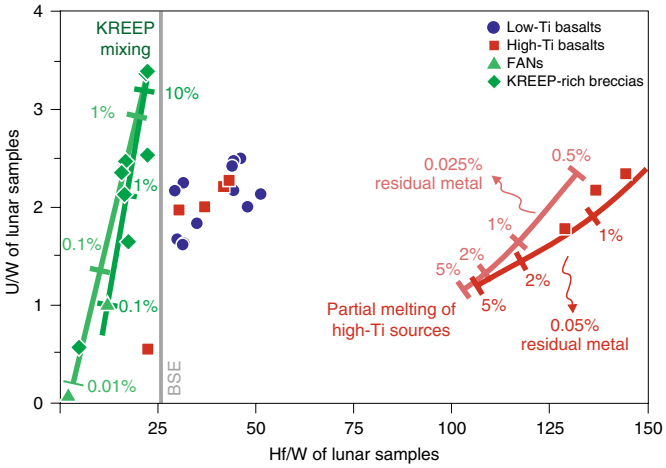

Fig. 1 | New U/W versus Hf/W data measured in lunar samples compared to crystallization and melting models for the LMO[35]. Errors are less than the symbol sizes. Measured lunar highland breccia compositions straddle the mixing lines between a KREEP-enriched end member[32] and FAN compositions as determined in this study. Contamination with W-rich meteoritic components produces virtually identical trajectories and raises the absolute W content. The high-Ti mare basalt source mineral assemblage is defined by a mixture of LMO cumulates that match Apollo 17 mare basalt Hf and Nd isotope systematics[12,27,32–35]. Note the overall excess of Hf/W in lunar basalts compared to recent BSE estimates[23].

sample suite that covers most relevant lithological units on the lunar nearside. Our samples include low- and high-Ti basalts, ferroan anorthosites (FANs) and KREEP-rich rocks. As shown in Fig. 1, these groups of samples are compositionally distinct, as expected from radiogenic isotope evidence and geochemical modelling[35]. Low-Ti mare basalts display a narrow range in U/W and Hf/W ratios, between 1.5 and 2.5 and between 30 and 50, respectively. In contrast, high-Ti basalts have Hf/W ratios as high as 150, and slightly more fractionated U/W, with values between 0.5 and 2.2. Finally, the KREEP-rich rocks and FAN samples exhibit the lowest Hf/W range of the studied sample suite, between ~5 (FAN) and 23 (KREEP rich), whereas their U/W shows the largest range among all the samples, with values that approach zero for FAN and are as high as 3.5 for the KREEP-rich rocks.

Lunar source modelling

Several key observations can be derived from our high-precision W–U–Th–HFSE data. For example, when combined, the FAN and KREEP-rich rocks form a clear linear array in Hf/W ratio versus U/W space (Fig. 1). This array can be directly linked to early lunar crust formation, that is, it is probably the result of mixing between a FAN end-member that has an exceedingly low Hf/W and U/W, and a KREEP-like component that has an elevated U/W and a Hf/W of around 20 (that is, lower than that of both the bulk silicate Moon (BSM) and the Earth's mantle). Interestingly, our results for these KREEP-rich samples corroborate previously modelled U/W and Hf/W values for KREEP using a fo_2-sensitive set of partition coefficients[32], which predicted that KREEP has an elevated U/W and a lower Hf/W ratio value than those of the BSM depending on fo_2. Our data thus show that the LMO crystallization model[36], as well as the mineral/melt partitioning data[24,25] used here, are sufficiently robust to mass balance these elements.

Our new results for lunar mare basalts have the best potential to constrain the Hf/W ratio of the silicate Moon. In defining which lunar mantle reservoirs of LMO cumulates were involved in the genesis of mare basalts, radiogenic Hf–Nd isotope data are the most powerful proxies to constrain their source mineral assemblages[35]. These assemblages allow us to model the geochemical relation between basalt and mantle compositions for the trace elements of interest. For example, Hf–Nd isotope data can clearly identify late-crystallizing mare basalt sources that comprise Ti-rich oxide phases and clinopyroxene, a characteristic that is absent from low-Ti mare basalt source regions[35]. Even at the low fo_2 of the lunar mantle, such oxide phases and clinopyroxene preferentially incorporate Hf over W and U (refs. [33,37]). Moreover, the mantle source of the Apollo 17 high-Ti mare basalts is the most likely lunar mantle source to contain residual metal during partial melting, owing to its reduced nature[32,33]. The residual metal in lunar mantle sources would undoubtedly retain W and not Hf, and thus generate a higher Hf/W ratio in coexisting mare basalts. When modelling high-Ti mare basalts with small fractions of residual metal, the high-Ti samples that exhibit the highest Hf/W ratios in our sample suite are perfectly reproduced (red melting curves in Fig. 1). The extreme Hf/W ratios displayed by Apollo 17 high-Ti mare basalts, and their covariation with U/W (Fig. 1), therefore directly reflect the combined effects of residual Ti-rich oxides, pyroxene and metal in the mantle sources of Apollo 17 high-Ti basalts. An unfortunate consequence of this feature is that any inferred U–W–Hf pattern strongly depends on the degree of partial melting, which is not well constrained for Apollo 17 basalts. Thus, Apollo 17 high-Ti mare basalts cannot be reliably used to infer the Hf/W ratio of the BSM, as done previously[18].

In contrast to the sample types above, the sources of low-Ti mare basalts are straightforward to model, as these are not overprinted by KREEP components and are essentially devoid of both Ti-rich oxides and metal[35] that may fractionate W from U, Th or HFSE. Moreover, low-Ti basalts are thought to result from higher degrees of partial melting compared to high-Ti basalts[38–41], and the U/W and Hf/W ratios measured in these basalts should be virtually identical to those in their respective sources. Interestingly, there are clearly resolvable differences between the different groups of low-Ti basalt samples (Fig. 1). This heterogeneity in Hf/W and U/W ratios in distinct low-Ti mantle sources is in perfect agreement with the isotopic heterogeneity documented by previously published Hf–Nd isotope data[35]. Moreover, the variations in Hf/W and U/W ratios observed in our lunar samples are consistent with previous experimental studies that predict that W is less incompatible than Hf during LMO crystallization and the partial melting of lunar mantle cumulates[32,33].

The mafic cumulates that constitute the mantle sources of low-Ti basalts are expected to preferentially retain W over Hf and U during LMO crystallization at reducing conditions (crystal/silicate melt partitioning values are given in the Supplementary Information). Therefore, the LMO cumulates and, by inference, the measured Hf/W ratios of low-Ti lunar mantle sources (30.2–48.7) record minimum estimates of the Hf/W ratio in the bulk LMO as well as in the silicate Moon. Our data show that the Hf/W ratio of the silicate Moon would lie between 30.2 and 48.5, clearly higher than the value estimated for the BSE (25.8 ± 2.6) (ref. [23]). As the addition of late veneer material would lower the lunar Hf/W ratio, the minimum estimate of the Hf/W ratio remains a robust one, being still resolvably higher than the Hf/W ratio of the BSE. In summary, low-Ti mare basalts allow the most reliable Hf/W ratio estimates in the lunar mantle, and the Hf/W ratio of the lunar mantle can be clearly shown to be resolvably higher than that of the Earth's mantle.

Lunar formation scenarios

Figure 2 illustrates three scenarios that can explain the higher Hf/W in the lunar mantle. A first, traditional, scenario (Fig. 2a) explains the different Hf/W ratios by variable proportions of added late veneer. It has been suggested in several studies[18–20] that the Moon received a considerably lower proportion of late veneer than the

BSE. The lower $\mu^{182}W$ and Hf/W ratio of the BSE are then explained by the addition of a higher amount of unradiogenic W through the late accretion to the Earth than that to the Moon. In a second scenario (Fig. 2b), the Moon-forming event could have taken place amidst ongoing terrestrial core formation, when ^{182}Hf was still present. If the Moon formed that early, core formation certainly took place in more-reducing conditions than during its final stages[41,42]. Under such more-reductive conditions, the Hf/W ratio of the BSE at the time of the giant impact would have been higher than at present, because W would have been more efficiently extracted into the growing core[41]. This model obviates the need for late accretion to explain the lunar excess in $\mu^{182}W$, because the Moon preserved a higher Hf/W ratio than the silicate Earth, which leads to less radiogenic $\mu^{182}W$ in the BSE and more radiogenic $\mu^{182}W$ in the silicate Moon. In the third scenario (Fig. 2c), core formation in the Moon could have scavenged sufficient W into the lunar core to elevate the Hf/W ratio of the BSM to its higher present-day value. This process has been invoked previously to explain the depletion of Cr and siderophile elements in the lunar mantle[43,44], with additional losses through evaporation[45]. If the lunar core and, by inference, the Moon formed while ^{182}Hf was extant, the silicate Moon would inevitably develop ^{182}W values higher than the present-day terrestrial value. Collectively, the latter two scenarios imply that late accretion was either of no consequence to the W budget and isotope composition of the silicate Moon, or that it was contemporaneous to the Moon-forming event.

A simple strategy to further evaluate the three models described above is to test the simplest hypothesis to explain why the Hf/W ratio of the silicate Moon is higher than that of BSE, that is, lunar core formation (the third scenario). If lunar core formation raises the Hf/W ratio of the silicate Moon to values as high as those shown here (that is, 30–50), then the first two hypotheses are potentially superfluous. Although there is plenty of evidence that the Moon has a small core, its exact composition and formation conditions are not well understood. However, the mass of the lunar core is much better constrained. Based on a recent re-evaluation of lunar seismic data[46–48], the lunar core comprises 1–3% of the total mass of the Moon. The question remains whether such a small core could have scavenged sufficient W to shift the Hf/W ratio of the silicate Moon to values as high as reported here. A simple mass balance[49] can be made to model the Hf/W ratio of the silicate Moon after lunar core formation. This model assumes that Hf is perfectly lithophilic and that its abundance in the bulk Moon and the BSE are identical. The Hf–W contents of the modelled silicate Moon can be calculated assuming a closed-system core formation over a range of realistic $D_W^{core/mantle}$ (15–100)[48], an initial Hf/W ratio of the BSE of 25.8 and different core mass fractions (1–3%)[46–48]. We also include a historical, lower estimate for the BSE[50]. The modelling results are depicted in Fig. 3, which shows that lunar core formation can, indeed, reproduce the range of the Hf/W ratio of the lunar mantle if one assumes a $D_W^{core/mantle}$ higher than 60, and a core mass fraction of at least 1.5%, that is, in line with recent estimates[46–48]. A more massive core (3% mass fraction) permits a smaller $D_W^{core/mantle}$ (~30) to reproduce the Hf/W ratio range of 30–50 reported here. It is thus clear from the results of this model that lunar core formation can viably generate the Hf/W ratio of the BSM using realistic values of $D_W^{core/mantle}$ and core mass fractions[49].

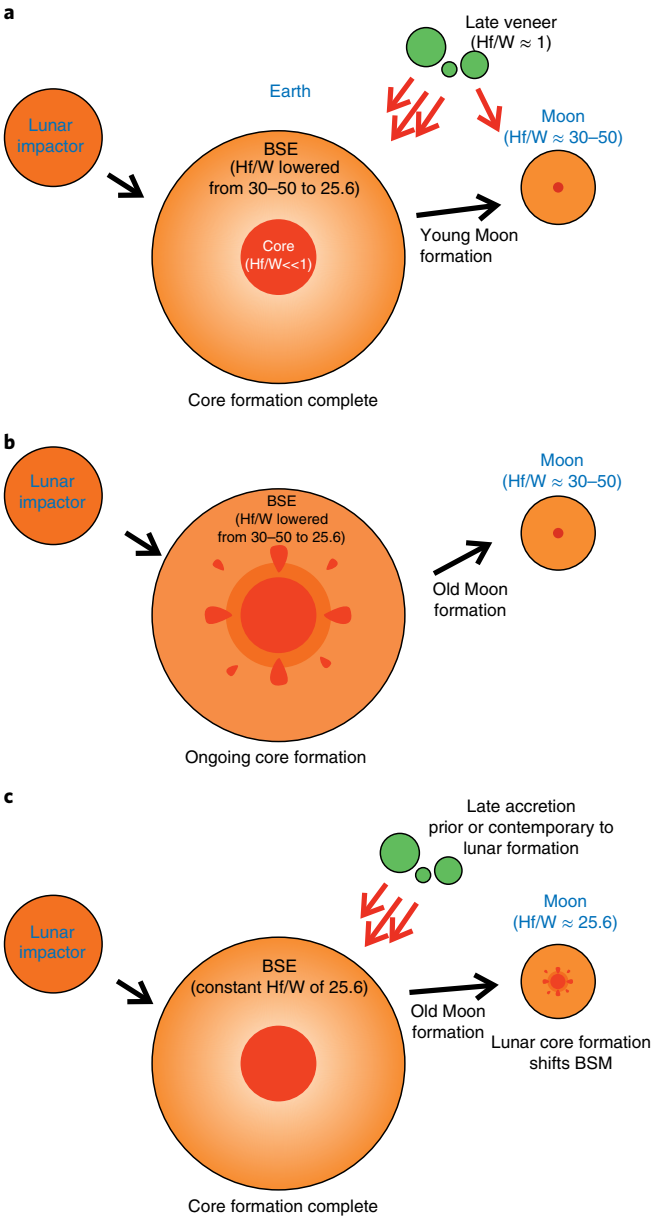

Fig. 2 | Scenarios that account for the higher Hf/W of the BSM. a, A late veneer of chondritic material (Hf/W ratio ≈1) lowers the BSE Hf/W from ~30–50 to 25.6 after ^{182}Hf extinction, whereas the Moon preserves its original Hf/W. **b**, The Moon-forming event takes place while Earth's core is still forming and ^{182}Hf is extant. Increasingly oxidizing conditions later lower the BSE Hf/W. **c**, The formation of a small lunar core scavenged W from the BSM, which increased its Hf/W. In models **b** and **c** the formation of the Moon must have occurred during the lifetime of ^{182}Hf, that is, within 60 Myr after the SSF.

Implications for dating lunar formation

Although the presence of a lunar core helps settle the ^{182}W excess, there remains evidence from other radiometric dating systems for a 'young Moon'. Evidence from direct measurements, such as zircons and FAN ages, can provide a younger age, but may be long offset from the parent body age[13–15,24]. Among these, our suggested age concurs with the oldest age found via U–Pb, at 4.51 billion years ago (Ga)[7]. Other methods, such as Sm–Nd model ages, indicate a young age for lunar crust formation, varying from 4.35 to 4.45 Ga, based on lunar basalts[15] and KREEP[13,17]. However, the age implied by these samples is for lunar crust formation, rather than for lunar formation. Importantly, the Sm–Nd model ages can represent post-formation mantle processes, which may have reset the different isotope systems.

In conclusion, we prefer a simple model for the lunar Hf–W patterns, wherein the difference in the Hf/W ratios between the silicate Moon and the silicate Earth is the result of lunar core formation. Figure 4 illustrates variations of lunar ^{182}W systematics as a function

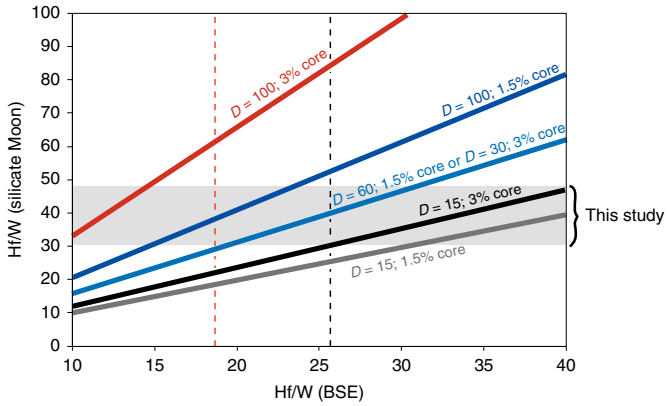

Fig. 3 | The effect of lunar core formation on the Hf/W ratio of the silicate Moon. The models assume different metal–silicate partition coefficients for W ($D_W^{core/mantle}$ between 15 and 100), and different lunar core mass fractions (1.5–3%). The initial Hf/W of the bulk Moon is the same as that of the BSE. The lunar Hf/W ratio value is reached with $D_W^{core/mantle}$ values between 30 and 60, and core mass fractions between 1.5 and 3% of the mass of the Moon. The two estimates of the BSE Hf/W encompass a historical value[50] (red dashed line) and a revised value based on high-precision measurements of Ta and W (ref. [23]) (black dashed line).

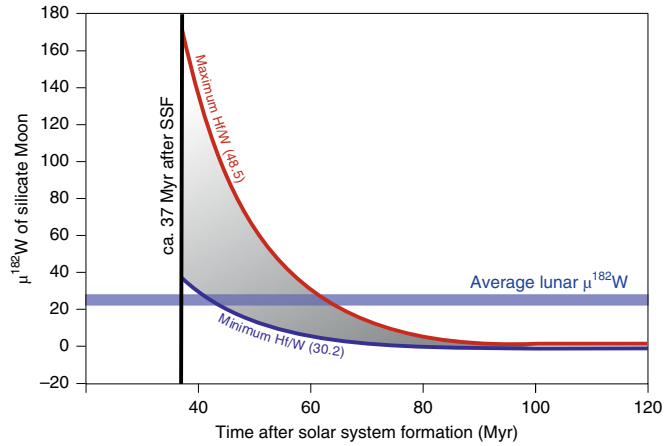

Fig. 4 | Tungsten isotope composition ($\mu^{182}W$) of the silicate Moon as a function of the lunar Hf/W ratio and formation age. Measured low-Ti mare basalt proxy for the range of the BSM Hf/W. The intersection with the mean reported BSM pre-exposure $\mu^{182}W$ provides the age interval following SSF for lunar formation to explain its $\mu^{182}W$ difference to that of Earth by the in situ decay of ^{182}Hf. The aggregated $\mu^{182}W$ is from Kruijer and Kleine[18]. The starting age of the curves (37 Myr) is taken from König et al.[23], as core formation ages from protracted core formation or incomplete equilibration models yield a younger age than this.

of the Hf/W ratio and age. The range of the Hf/W ratios measured in our study, combined with recent estimates for the lunar $\mu^{182}W$, requires lunar differentiation to have occurred between 40 and ~60 Myr after SSF. We can thus unambiguously relate the ^{182}W excess in lunar samples to the in situ decay of ^{182}Hf to ^{182}W. The combination of a robust set of experimental partitioning data with a high-precision HFSE analysis is thus both in favour of an 'old Moon' and diminishes the role of late accretion in creating the $\mu^{182}W$ signature of the Moon. In addition to helping settle the ongoing strife between 'old' and 'new' Moon scenarios, this method can also be used to unravel the formation timescales of other planetary bodies, which is of key importance to future sample return missions.

Online content

Any methods, additional references, Nature Research reporting summaries, source data, statements of code and data availability and associated accession codes are available at https://doi.org/10.1038/s41561-019-0398-3.

Received: 22 January 2019; Accepted: 4 June 2019;
Published online: 29 July 2019

References

1. Canup, R. M. Forming a moon with an Earth-like composition via a giant impact. *Science* **338**, 1052–1055 (2012).
2. Melosh, H. J. New approaches to the Moon's isotopic crisis. *Phil. Trans. Royal Soc. A* **372**, 20130168 (2014).
3. Zhang, J., Dauphas, N., Davis, A. M., Leya, I. & Fedkin, A. The proto-Earth as a significant source of lunar material. *Nat. Geosci.* **5**, 251–255 (2012).
4. Weyer, S. et al. Iron isotope fractionation during planetary differentiation. *Earth Planet. Sci. Lett.* **240**, 251–264 (2005).
5. Armytage, R., Georg, R., Williams, H. & Halliday, A. Silicon isotopes in lunar rocks: implications for the Moon's formation and the early history of the Earth. *Geochim. Cosmochim. Acta* **77**, 504–514 (2012).
6. Dauphas, N., Burkhardt, C., Warren, P. H. & Fang-Zhen, T. Geochemical arguments for an Earth-like Moon-forming impactor. *Phil. Trans. Royal Soc. A* **372**, 20130244 (2014).
7. Barboni, M. et al. Early formation of the Moon 4.51 billion years ago. *Sci. Adv.* **3**, e1602365 (2017).
8. Jacobson, S. A. et al. Highly siderophile elements in Earth's mantle as a clock for the Moon-forming impact. *Nature* **508**, 84–87 (2014).
9. Yin, Q.-Z. et al. Records of the Moon-forming impact and the 470 Ma disruption of the L chondrite parent body in the asteroid belt from U–Pb apatite ages of Novato (L6). *Meteorit. Planet. Sci.* **49**, 1426–1439 (2014).
10. Bottke, W. et al. Dating the Moon-forming impact event with asteroidal meteorites. *Science* **348**, 321–323 (2015).
11. Yin, Q. et al. A short timescale for terrestrial planet formation from Hf–W chronometry of meteorites. *Nature* **418**, 949–952 (2002).
12. Moynier, F. et al. Coupled ^{182}W–^{142}Nd constraint for early Earth differentiation. *Proc. Natl Acad. Sci. USA* **107**, 10810–10814 (2010).
13. Carlson, R. W., Borg, L. E., Gaffney, A. M. & Boyet, M. Rb–Sr, Sm–Nd and Lu–Hf isotope systematics of the lunar Mg-suite: the age of the lunar crust and its relation to the time of Moon formation. *Phil. Trans. Royal Soc. A* **372**, 20130246 (2014).
14. Connelly, J. & Bizzarro, M. Lead isotope evidence for a young formation age of the Earth–Moon system. *Earth Planet. Sci. Lett.* **452**, 36–43 (2016).
15. Borg, L. E., Connelly, J. N., Boyet, M. & Carlson, R. W. Chronological evidence that the Moon is either young or did not have a global magma ocean. *Nature* **477**, 70–72 (2011).
16. Snape, J. F. et al. Lunar basalt chronology, mantle differentiation and implications for determining the age of the Moon. *Earth Planet. Sci. Lett.* **451**, 149–158 (2016).
17. Borg, L. E., Gaffney, A. M. & Shearer, C. K. A review of lunar chronology revealing a preponderance of 4.34–4.37 Ga ages. *Meteorit. Planet. Sci.* **50**, 715–732 (2015).
18. Kruijer, T. S. & Kleine, T. Tungsten isotopes and the origin of the Moon. *Earth Planet. Sci. Lett.* **475**, 15–24 (2017).
19. Kruijer, T. S., Kleine, T., Fischer-Gödde, M. & Sprung, P. Lunar tungsten isotopic evidence for the late veneer. *Nature* **520**, 534–537 (2015).
20. Touboul, M., Puchtel, I. S. & Walker, R. J. Tungsten isotopic evidence for disproportional late accretion to the Earth and Moon. *Nature* **520**, 530–533 (2015).
21. Vockenhuber, C. et al. New half-life measurement of ^{182}Hf: improved chronometer for the early solar system. *Phys. Rev. Lett.* **93**, 172501 (2004).
22. Münker, C. A high field strength element perspective on early lunar differentiation. *Geochim. Cosmochim. Acta* **74**, 7340–7361 (2010).
23. König, S. et al. The Earth's tungsten budget during mantle melting and crust formation. *Geochim. Cosmochim. Acta* **75**, 2119–2136 (2011).
24. Rizo, H. et al. Preservation of Earth-forming events in the tungsten isotopic composition of modern flood basalts. *Geochim. Cosmochim. Acta* **175**, 319–336 (2016).
25. Willbold, M., Elliott, T. & Moorbath, S. The tungsten isotopic composition of the Earth's mantle before the terminal bombardment. *Nature* **477**, 195–198 (2011).
26. Puchtel, I. S., Blichert-Toft, J., Touboul, M., Horan, M. F. & Walker, R. J. The coupled ^{182}W–^{142}Nd record of early terrestrial mantle differentiation. *Geochem. Geophys. Geosys.* **17**, 2168–2193 (2016).
27. Mundl, A. et al. Tungsten-182 heterogeneity in modern ocean island basalts. *Science* **356**, 66–69 (2017).

28. Jones, T. D., Davies, D. R. & Sossi, P. A. Tungsten isotopes in mantle plumes: heads it's positive, tails it's negative. *Earth Planet. Sci. Lett.* **506**, 255–267 (2019).
29. Puchtel, I. S., Blichert-Toft, J., Touboul, M. & Walker, R. J. ^{182}W and HSE constraints from 2.7 Ga komatiites on the heterogeneous nature of the Archean mantle. *Geochim. Cosmochim. Acta* **228**, 1–26 (2018).
30. Tusch, J. et al. Uniform ^{182}W isotope compositions in Eoarchean rocks from the Isua region, SW Greenland: the role of early silicate differentiation and missing late veneer. *Geochim. Cosmochim. Acta* **257**, 284–310 (2019).
31. Palme, H. & Rammensee, W. The significance of W in planetary differentiation processes: evidence from new data on eucrites. *Proc. Lunar Planet. Sci.* **12**, 949–964 (1982).
32. Fonseca, R. O. C. et al. Redox controls on tungsten and uranium crystal/silicate melt partitioning and implications for the U/W and Th/W ratio of the lunar mantle. *Earth Planet. Sci. Lett.* **404**, 1–13 (2014).
33. Leitzke, F. L. et al. The effect of titanium on the partitioning behavior of high-field strength elements between silicates, oxides and lunar basaltic melts with applications to the origin of mare basalts. *Chem. Geol.* **440**, 219–238 (2016).
34. Leitzke, F. P. et al. Redox dependent behaviour of molybdenum during magmatic processes in the terrestrial and lunar mantle: implications for the Mo/W of the bulk silicate Moon. *Earth Planet. Sci. Lett.* **474**, 503–515 (2017).
35. Sprung, P., Kleine, T. & Scherer, E. E. Isotopic evidence for chondritic Lu/Hf and Sm/Nd of the Moon. *Earth Planet. Sci. Lett.* **380**, 77–87 (2013).
36. Snyder, G. A., Taylor, L. A. & Neal, C. R. A chemical model for generating the sources of mare basalts: combined equilibrium and fractional crystallization of the lunar magmasphere. *Geochim. Cosmochim. Acta* **56**, 3809–3823 (1992).
37. Dygert, N., Liang, Y. & Hess, P. The importance of melt TiO_2 in affecting major and trace element partitioning between Fe–Ti oxides and lunar picritic glass melts. *Geochim. Cosmochim. Acta* **106**, 134–151 (2013).
38. Day, J. M. & Walker, R. J. Highly siderophile element depletion in the Moon. *Earth Planet. Sci. Lett.* **423**, 114–124 (2015).
39. Day, J. M., Pearson, D. G. & Taylor, L. A. Highly siderophile element constraints on accretion and differentiation of the Earth–Moon system. *Science* **315**, 217–219 (2007).
40. Day, J., Puchtel, I., Walker, R., James, O. & Taylor, L. Osmium abundance and isotope systematics of lunar crustal rocks and mare basalts. *Lunar Planet. Sci. Conf.* **39**, 1071 (2008).
41. Wade, J. & Wood, B. J. Core formation and the oxidation state of the Earth. *Earth Planet. Sci. Lett.* **236**, 78–95 (2005).
42. Wood, B., Walter, M. & Wade, J. Accretion of the Earth and segregation of its core. *Nature* **441**, 825–833 (2006).
43. Walter, M., Newsom, H., Ertel, W., Holzheid, A. in *Origin of the Earth and Moon* (eds Canup, R. M. & Righter, K) 265–289 (Univ. Arizona Press, 2000).
44. Steenstra, E., Rai, N., Knibbe, J., Lin, Y. & van Westrenen, W. New geochemical models of core formation in the Moon from metal–silicate partitioning of 15 siderophile elements. *Earth Planet. Sci. Lett.* **441**, 1–9 (2016).
45. Sossi, P. A., Moynier, F. & van Zuilen, K. Volatile loss following cooling and accretion of the Moon revealed by chromium isotopes. *Proc. Natl Acad. Sci. USA* **115**, 10920–10925 (2018).
46. Weber, R. C., Lin, P.-Y., Garnero, E. J., Williams, Q. & Lognonne, P. Seismic detection of the lunar core. *Science* **331**, 309–312 (2011).
47. Khan, A., Pommier, A., Neumann, G. & Mosegaard, K. The lunar moho and the internal structure of the Moon: a geophysical perspective. *Tectonophysics* **609**, 331–352 (2013).
48. Garcia, R. F., Gagnepain-Beyneix, J., Chevrot, S. & Lognonné, P. Very preliminary reference Moon model. *Phys. Earth Planet. Int.* **188**, 96–113 (2011).
49. Rai, N. & van Westrenen, W. Lunar core formation: new constraints from metal–silicate partitioning of siderophile elements. *Earth Planet. Sci. Lett.* **388**, 343–352 (2014).
50. Newsom, H. et al. The depletion of tungsten in the bulk silicate earth: constraints on core formation. *Geochim. Cosmochim. Acta* **60**, 1155–1169 (1996).

Acknowledgements

M.M.T. and C.M. acknowledge funding through the European Commission by ERC grant 669666 'Infant Earth'. M.M.T. acknowledges funding from Deutsche Forschungsgemeinschaft (DFG) Projekt no. 213793859 (SP 1385/1-1 to P.S.) and EoS project ET-HOME (present funding); R.O.C.F. acknowledges funding for a Heisenberg Fellowship by the DFG through grant DFG FO 698/5-1 and FO 698/6-1; P.S. acknowledges funding from UoC emerging fields grant 'ULDETIS'. F.P.L. acknowledges funding for a PhD scholarship by DAAD/CNPq (248562/2013-4). F. Wombacher and the Cologne/Bonn support staff are thanked for laboratory operations. C.D. Garbe-Schönberg (CAU zu Kiel) is thanked for the conventional trace element analyses. CAPTEM is thanked and acknowledged for sample allocations.

Author contributions

M.M.T. and C.M. did the sample digestions, column chemistry and HFSE–W–U–Th isotope dilution concentration measurements partially supported by P.S. on the Neptune MC-ICP-MS. P.S., R.O.C.F. and F.P.L. did the modelling based on experimental partitioning data. M.M.T. did the modelling that related Hf/W to ^{182}W. All the authors contributed towards the writing of the manuscript and the discussion of the implications of the data.

Competing interests

The authors declare no competing interests.

Additional information

Supplementary information is available for this paper at https://doi.org/10.1038/s41561-019-0398-3.

Reprints and permissions information is available at www.nature.com/reprints.

Correspondence and requests for materials should be addressed to M.M.T.

Publisher's note: Springer Nature remains neutral with regard to jurisdictional claims in published maps and institutional affiliations.

Methods

Sample selection. Samples were provided by the Curation and Analysis Planning Team for Extraterrestrial Materials and selected to represent the major lithological units of the Moon as sampled by the NASA Apollo missions. To characterize their chemical composition, our particular focus lay on the quantification of any inherent U/W, Th/W and Hf/W variability as inferred from the few previous studies available. Some sample duplicity with previous studies allowed for an additional quality assessment. In total, lunar samples from Apollo 11 (three), Apollo 12 (six), Apollo 14 (three), Apollo 15 (six), Apollo 16 (four) and Apollo 17 (four) were analysed. Of these, seven were Apollo 11 or Apollo 17 high-Ti mare basalts and soils, 14 were low-Ti mare basalts from Apollo 12 and Apollo 15, two were Apollo 16 FANs, along with seven KREEP-rich samples, which included a meteorite and KREEP-rich breccias and KREEP basalts from the Apollo 14, 16 and 17 missions.

Sample preparation. To obtain high-precision data, we measured all the elements of interest by isotope dilution and added several isotope tracers to ~100 mg (250 mg for anorthosites) of each sample prior to digestion. The mixed isotope tracers included ^{229}Th–^{233}U–^{236}U and ^{183}W–^{180}Ta–^{180}Hf–^{176}Lu–^{94}Zr mixed solutions. Samples were digested in 3 ml of double distilled HF and 3 ml of distilled HNO_3 for 24 h at 120 °C. Prior to drydown, 0.5 ml of perchloric acid were added to ensure a sample-spike equilibrium for Th. Samples were redissolved with concentrated HNO_3 and trace HF to ensure the redissolution of HFSE. These sample solutions were subsequently dried down again, and redissolved in 6 ml of 6 M HCl–0.06 M HF to ensure a full sample-spike equilibrium for HFSE. These samples were then aliquoted, with 10% of the solution used for conventional trace element analysis, 20% for W isotope dilution measurements and 70% for high-field-strength and U–Th element analysis. For a first batch of samples, an additional aliquot of 10% for U–Th was taken. The anorthosite samples were aliquoted with 85% for a combined HFSE, W and U–Th aliquot, and 15% for trace element analysis.

The trace element aliquot was dried down, dissolved in concentrated HNO_3 and then dried down again. This residue was subsequently dissolved in 1 ml of concentrated HNO_3, with 4 ml of MilliQ H_2O added, and then diluted with MilliQ H_2O to 50 ml. Conventional trace element analyses on these aliquots were performed at the Quadrupole ICP-MS laboratory at the Institut für Geowissenschaften at CAU zu Kiel using the procedure of Garbe-Schönberg[51].

Our protocol to separate individual HFSE and U–Th cuts from lunar samples is a modified protocol based the literature[22,52,53]. During the protocol, individual cuts that contained a matrix, heavy rare earth elements (HREEs), Zr–Nb, Ta, Hf and U–Th were separated from the HFSE aliquot. Tungsten was separated from the W isotope dilution step via a separate set of anion-exchange resin microcolumns (Table 4 in Kleine et al.[53]).

In our HFSE protocol, the sample aliquots were dissolved in 3M HCl and loaded onto a Ln Spec resin column. Matrix and light REEs were eluted in 3 M HCl. An HREE fraction that contained the most Lu was eluted with 6M HCl, followed by elution of an HFSE cut that contained Ti–Zr–Nb–Hf–Ta–U–Th in 2M HF. A quantitative Zr/Nb aliquot was taken from this fraction[52]. The remaining HFSE cut was loaded onto a Bio-Rad column that contained an AG 1×8 100–200 mesh resin. The U–Th fraction was collected in 2M HF, and a Ti–Zr–Hf fraction was collected in 6M HNO_3/0.2M HF. A clean Ta fraction was subsequently collected in 6M HNO_3/0.2M HF/1% H_2O_2. The Ti–Zr–Hf fraction was dried down overnight and loaded onto the stage I Ln Spec resin column in 3M HCl. After clean-up in 6M HCl and MilliQ H_2O, Ti was eluted using a 1M HNO_3–2% H_2O_2 mixture[54] and some Zr was eluted in 6M HCl—0.06M HF. Hafnium was finally eluted in 2M HF.

Separation of U–Th was performed in two ways, following a modified literature protocol[55]. For the first batch of samples, a full aliquot was used, whereas for the other batches the U–Th fraction from the 2M HF elution step above was taken. After drydown, the U- and Th-bearing cuts were dissolved in 1.5M HNO_3, before being loaded onto columns that contained TRU-Spec resin (200–400 mesh). In a modification of the chemistry of Luo et al.[55], all the major elements were initially eluted in 1.5M HNO_3. After the removal of the rare earth elements in 3M HCl, Th was eluted in 0.2M HCl. Finally, U was eluted in 0.1M HCl/0.3M HF.

Given the low concentrations of the elements of interest in anorthosites, we performed a different separation protocol for these samples. About 70% of the 85% HFSE aliquots of anorthosites was loaded on an anion exchange resin in 1M HCl/0.5M HF solution. The eluted matrix cut and an additional fraction rinsed in 0.5M HCl/0.5M HF contained most of the Rb–Sr, Sm–Nd and U–Th. A fraction that contained Ti–Zr–Hf was collected in 6M HCl/0.06M HF, from which Hf was further purified using Ln Spec resin (see above). A W fraction was subsequently eluted in 6M HNO_3/0.2M HF, followed by Ta elution in 6M HNO_3/0.2M HF/1% H_2O_2. After drydown, the Ta cut was loaded again on the same anion resin column for clean-up, and the Ta was again eluted in 6M HNO_3/0.2M HF/1% H_2O_2 after clean-up in 6M HNO_3/0.2M HF. The remaining 15% of the anorthosite HFSE aliquots was loaded on Ln Spec resin in 3M HCl. Two fractions that contained HREE and Zr/Nb were eluted from the column in 6M HCl and 2M HF, as described above. The advantage of this approach is that a larger W fraction is collected, which thus avoids low sample-to-blank ratios during W isotope dilution measurements.

Analytical protocols. All the isotope dilution measurements were performed using the Neptune MC-ICP-MS at the University of Cologne. Detailed descriptions of the analytical protocols for the HFSE measurements, analytical uncertainties and further references are given in Münker[22]. For ^{229}Th/^{232}Th measurements, we used a secondary electron multiplier ion counter equipped with an RPQ system on mass ^{229}Th. The Th cuts were doped with the NBL CRM 112A U standard for a mass bias correction, and the ion counter was calibrated with concentration-matched IRM-035 and IRM 036 standards for ion counter yield corrections. For U measurements, mass bias was corrected using the measured ^{233}U/^{236}U of the spiked U cuts and the certified ^{233}U/^{236}U from Richter et al.[56] for the doped IRM-3636 double spike used for preparation of the mixed U–Th tracer. Our external precision and accuracy for elemental ratios determined by isotope dilution that involved U and Th was typically better than ±1% for both U/W and Th/W (2σ relative standard deviation). Typical blanks used during the course of the measurements were below 50 pg for W, 66 pg for U, 32 pg for Th and 30 pg for Hf. These blanks proved negligible, with total a blank uncertainty, including propagated errors, of less than ±1%.

Results (and modelling constraints). The measured HFSE and HFSE/U–Th ratios were distinct for different sample groups and mineralogy, with only small variations in U/W and Hf/W between samples from the same lithology. High-Ti basalts are particularly heterogeneous, with samples from the three measured localities that showed distinct Hf/W and U/W values. Apollo 17 high-Ti breccias both have similar values, with Hf/W ranging from 31 to 35, at a constant U/W of 1.9. This is distinct from Apollo 17 high-Ti mare basalts, for which U/W correlates positively with Hf/W. The Apollo 11 high-Ti mare basalts both have Hf/W of 42 and U/W of 2.2. Unique among all the samples are the Apollo 17 high-Ti mare basalts, which bear exceptionally high Hf/W ratios, between 120 and 150. Likewise, the low-Ti basalts plot as particularly distinctive groups according to the mission site. The Apollo 12 ilmenite basalts have a similar U/W to those of the Apollo 12 olivine and pigeonite basalts, of 2.07 and 2.25, respectively. However, they are distinct in their Hf/W, with both pigeonite-bearing basalts near 30 and ilmenite basalts of 43–48. The Apollo 15 quartz-normative and olivine-normative low-Ti basalts have different U/W, ranging from an average of 2.45 in the former to 1.75 in the latter. The Hf/W ratios of the two low-Ti basalt groups also vary from 45 (quartz-normative) to 30 (olivine normative). Whereas the olivine-normative low-Ti basalts of both Apollo 15 and Apollo 12 have identical Hf/W, their U/W differ significantly, from among the lowest values (1.63) measured to the highest (2.53), respectively. The KREEP-rich samples have a very narrow range in Hf/W of ~20. The U/W of KREEP samples has the largest spread, with most samples in the range 1.63 to 2.51, and minimum and maximum values of 0.54 and 3.38, respectively.

LMO fractionation and partial melting modelling. The LMO[57–59] crystallization model utilized in this study is based on the cumulate crystallization sequence of Snyder et al.[36]. We previously showed[32] that the results of this and other LMO crystallization models[60,61] are in good agreement. The same starting composition as used in Fonseca et al.[32] (after Münker[22]) was chosen to evaluate the general HFSE–W–U–Th systematics of a crystalizing LMO. For W, an additional mass balance between the estimate of its content in the BSM after core formation was done following Steenstra et al.[44] by considering different core mass fractions (1–3% of the total mass of the Moon). The LMO crystallization model was divided into four main steps: (1) equilibrium crystallization of olivine and orthopyroxene (until 78% solidification), (2) fractional crystallization of plagioclase, olivine and pigeonite (until 86% solidification), (3) fractional crystallization of clinopyroxene, plagioclase and pigeonite (until 95% solidification) and (4) crystallization of pigeonite, plagioclase, clinopyroxene and ilmenite (until 99.5% solidification). The remaining 0.5% after LMO crystallization is a liquid residue strongly enriched in incompatible trace elements and called urKREEP, which reflects its characteristic enrichments in K, REE and P (refs. [62,63]). The LMO crystallization model assumes that various amounts of trapped instantaneous residual liquid (that is, coexisting melt at the time of crystallization) are part of lunar mantle cumulates to take into account the major element variation observed in lunar mare basalts[36]. To account for the Al content of lunar basaltic samples[36], the model also considers that at the moment plagioclase appears on the liquidus, 98% of the crystallizing plagioclase floated to the uppermost portion of the LMO to form the lunar crust with only 2% being entrained in the cumulates. After LMO crystallization, the layered lunar mantle underwent a density-driven mantle overturn which mixed the different cumulate layers to produce new hybrid mantle domains that served as the source for partial melts that crystallized to form the lunar mare basalts[64]. To understand the implications of these processes for the trace element inventory of mare basalts thus involved aggregate modal fractional melting models of hybrid lunar mantle domains. The mixing proportions of different primary LMO cumulates in the hybridized lunar mantle sources, their mineral assemblages and the amount of trapped instantaneous residual liquid were constrained from the Lu–Hf and Sm–Nd isotope patterns of lunar basalts[35]. We also assumed that a small proportion of residual metal may be required at the lunar mantle source to reproduce the values observed for high-Ti basalts, which is in agreement with the extremely reduced nature of the lunar mantle and the depletion in Ni observed for lunar olivine[65,66]. For the purposes of our modelling we have assumed the LMO equilibrated at an fO_2 of about IW −1, in agreement with the current estimates of oxygen fugacity for

the lunar mantle[66,67]. Trace element crystal/silicate melt partition coefficients for different pyroxenes, plagioclase and olivine (Supplementary Information) were selected taking into account the variation of TiO_2 exhibited by lunar mare basalts and the changing composition of the LMO during crystallization[34] as well as the effect of fo_2 on the partitioning behaviour of W (refs. [32,33]). The ilmenite/silicate melt trace element partition coefficients are an average of the high-Ti experiments listed in Dygert et al.[37]). The liquid metal/silicate melt W partition coefficients are from Righter et al.[68] and Steenstra et al.[44], which cover a wide range of values (15–100)[48].

To calculate the age range for lunar formation, we defined the minimum and maximum Hf/W estimates for the BSM based on our measurements of low-Ti basalts. The value for the Hf/W of the BSE of 25.8 is taken from Konig et al.[23]. We define a $^{182}W/^{184}W$ of the BSE as 0.864863 (ref. [69]). Initial $^{182}Hf/^{180}Hf$ of 0.0001018 is from Kruijer et al.[70]. The $\lambda^{182}Hf$ is taken from Vockenhuber et al.[21]. Given these values, we calculate the necessary time of lunar formation as a function of ^{182}Hf decay for a given Hf/W ratio of the BSM in order to create the ^{182}W excess found on the Moon.

Data availability

The authors declare that the data supporting the findings of this study are available within the article and its Supplementary Information files.

References

51. Garbe-Schönberg, C.-D. Simultaneous determination of thirty-seven trace elements in twenty-eight international rock standards by ICP-MS. *Geostand. Geoanal. Res.* **17**, 81–97 (1993).
52. Münker, C., Weyer, S., Scherer, E. E. & Mezger, A. Separation of high field strength elements (Nb, Ta, Zr, Hf) and Lu from rock samples for MC-ICPMS measurements. *Geochem. Geophys. Geosyst.* **2**, 2001GC000183 (2001).
53. Kleine, T., Mezger, K., Palme, H. & Münker, C. The W isotope evolution of the bulk silicate Earth: constraints on the timing and mechanisms of core formation and accretion. *Earth Planet. Sci. Lett.* **228**, 109–123 (2004).
54. Bast, R. et al. A rapid and efficient ion-exchange chromatography for Lu–Hf, Sm–Nd, and Rb–Sr geochronology and the routine isotope analysis of sub-ng amounts of Hf by MC-ICP-MS. *J. Anal. Atom Spectrom.* **30**, 2323–2333 (2015).
55. Luo, X. M., Rehkämper, D.-C. & Lee, A. N. Halliday High precision $^{230}Th/^{232}Th$ and $^{234}U/^{238}U$ measurements using energy filtered ICP magnetic sector multiple collector mass spectrometry. *Int. J. Mass Spectrom. Ion. Process.* **171**, 105–117 (1997).
56. Richter, S. et al. New average values for the $n(^{238}U)/n(^{235}U)$ isotope ratios of natural uranium standards. *Int. J. Mass Spectrom.* **295**, 94–97 (2010).
57. Smith, J. V. et al. Petrologic history of the moon inferred from petrography, mineralogy, and petrogenesis of Apollo 11 rocks. *Geochim. Cosmochim. Acta* **34** (Suppl.), 897–925 (1970).
58. Warren, P. H. The magma ocean concept and lunar evolution. *Annu. Rev. Earth Planet. Sci. Lett.* **13**, 201–240 (1985).
59. Wood, J. A., Dickey, J. S., Marvin, U. B. & Powell, B. N. Lunar anorthosites and a geophysical model of the moon. *Geochim. Cosmochim. Acta* **34** (Suppl.), 965–988 (1970).
60. Elardo, S. M., Draper, D. S. & Shearer, C. K. Lunar magma ocean crystallization revisited: bulk composition, early cumulate mineralogy, and the source regions of the highlands mg-suite. *Geochim. Cosmochim. Acta* **75**, 3024–3045 (2011).
61. Elkins-Tanton, L. T., van Orman, J. A., Hager, B. H. & Grove, T. L. Re-examination of the lunar magma ocean cumulate overturn hypothesis: melting or mixing is required. *Earth Planet. Sci. Lett.* **196**, 239–249 (2002).
62. Meyer, C. Jr et al. Mineralogy, chemistry, and origin of the KREEP component in soil samples from the Ocean of Storms. In *Proc. 2nd Lunar Sci. Conf.* Vol 1 (ed. Levinson, A. A.) 393–411 (MIT, 1971).
63. Warren, P. H. & Wasson, J. T. The origins of KREEP. *Rev. Geophys.* **17**, 73–88 (1979).
64. Hess, P. C. & Parmentier, E. M. A model for the thermal and chemical evolution of the Moons interior: implications for the onset of mare volcanism. *Earth Planet. Sci. Lett.* **134**, 501–514 (1995).
65. Karner, J., Papike, J. J. & Shearer, C. K. Olivine from planetary basalts: chemical signatures that indicate planetary parentage and those that record igneous setting and process. *Am. Mineral.* **88**, 806–816 (2000).
66. Nicholis, M. & Rutherford, M. J. Graphite oxidation in the Apollo 17 orange glass magma: implications for the generation of a lunar volcanic gas phase. *Geochim. Cosmochim. Acta* **73**, 5905–5917 (2009).
67. Papike, J. J., Karner, J. M. & Shearer, C. K. Comparative planetary mineralogy: valence state partitioning of Cr, Fe, Ti, and V among crystallographic sites in olivine, pyroxene, and spinel from planetary basalts. *Am. Mineral.* **90**, 277–290 (2005).
68. Righter, K., Pando, K. M., Danielson, L. & Lee, C. T. Partitioning of Mo, P and other siderophile elements (Cu, Ga, Sn, Ni Co, Cr, Mn, V and W) between metal and silicate melt as a function of temperature and silicate melt composition. *Earth Planet. Sci. Lett.* **291**, 1–9 (2010).
69. Kleine, T. et al. Hf–W chronology of the accretion and early evolution of asteroids and terrestrial planets. *Geochim. Cosmochim. Acta* **73**, 5150–5188 (2009).
70. Kruijer, T., Kleine, T., Fischer-Gödde, M., Burkhardt, C. & Wieler, R. Nucleosynthetic W isotope anomalies and the Hf–W chronometry of Ca–Al-rich inclusions. *Earth Planet. Sci. Lett.* **403**, 317–327 (2014).